Mid-IR Amplification Based on a Pr^{3+}: InF_3 Optical Fiber in the Range $3.8 - 4.2\ \mu m$

Antonella Maria Loconsole, Vito Vincenzo Francione, Francesco Anelli, Stefano Taccheo, and Francesco Prudenzano, *Member, IEEE*

***Abstract*—In this article, for the first time, to the best of our knowledge, a fiber optic amplifier, operating in the middle-infrared wavelength range, has been designed, considering a single mode fluoroindate optical fiber, doped with praseodymium. After the electromagnetic investigation of the fiber, the design of the optical amplifier has been performed via a home-made computer code solver, employing measured spectroscopical parameters. The validated code solves the rate equation and the power propagation equation of the pump, the signal, and Amplifier Spontaneous Emission noise, considering the first and second order phenomena. The designed optical amplifier is very promising, exhibiting high simulated gain $G = 32.6$ dB and a wide -3 dB bandwidth of 115 nm with noise figure $NF = 6$ dB around the central signal wavelength $4\mu m$, for input pump power $P_p = 2$ W, input signal power $P_s = -30$ dBm, and pump wavelength $\lambda_p = 1.55\ \mu m$. This work suggests that high-performance Mid-IR optical amplifier could be fabricated considering feasible fluoroindate optical fiber doped with praseodymium providing for the first time the design parameters.**

***Index Terms*—Doped fiber amplifier, fluoroindate glass, mid-IR device, praseodymium, rare-earth doping.**

I. Introduction

THE exploitation of middle-infrared (Mid-IR) wavelength range promises high impact in different fields such as sensing, communication, medicine, and aerospace. Several devices have been proposed in this wavelength range such as continuous wave (CW) and pulsed lasers [1], [2], [3], [4], [5], [6], [7], [8], [9], [10], supercontinuum sources [11], [12], [13], sensors [14], [15], [16], and optical combiners [17], [18]. Their construction has been performed by employing different glasses such as fluoride, chalcogenide, and germanate ones [19], [20], [21]. In particular, in the last years, several Mid-IR fiber optical amplifiers have been experimentally demonstrated [22], [23], [24] or simulated [25], [26], [27], [28]. As examples, erbium-doped ZBLAN (Er^{3+}:ZBLAN) fiber amplifiers, with central wavelength $\lambda_s = 2.7\ \mu m$ [22]; high power and polarization maintaining optical amplifiers based on fluoride glass doped with erbium (Er^{3+}:ZFG) with central wavelength $\lambda = 2.8\ \mu m$ [23]; fluoride fibers doped with erbium (Er^{3+}:ZFG) for amplification of nanosecond pulses at $\lambda = 2.79\ \mu m$ [24]; chalcogenide fibers doped with praseodymium (Pr^{3+}:GeAsFaSe) for amplification at wavelength $\lambda = 4.3\ \mu m$ [25]; broadband amplifiers based on chalcogenide fiber doped with i) dysprosium (Dy^{3+}:GeAsFaSe), and ii) terbium (Tb^{3+}:GeAsFaSe) for amplification of ultrashort pulses [26]; Master Oscillator Power Amplifier (MOPA) based on a chalcogenide glass doped with dysprosium (Dy^{3+}:$Ga_5Ge_{20}Sb_{10}S_{65}$) with central wavelength $\lambda_s = 4.38\ \mu m$ [27]. Alternative solutions for amplification at central wavelength $\lambda_s = 2.77\ \mu m$ can be obtained coupling tapered fiber with microsphere, employing chalcogenide glass doped with erbium (Er^{3+}:$Ga_5Ge_{20}Sb_{10}S_{65}$) [28].

To the best of our knowledge, fluoride glasses doped with praseodymium have never been employed to obtain optical amplifiers working in Mid-IR range. Praseodymium-doped ZBLAN (Pr^{3+}:ZBLAN) glasses have been employed to design optical amplifiers working in the Near Infrared (NIR) range [29], [30], [31].

In this paper, for the first time, a Mid-IR optical amplifier based on a praseodymium-doped fluoroindate glass (Pr^{3+}:InF_3), working at central wavelength $\lambda_s = 4\ \mu m$ is designed and optimized. The parameters useful for the fabrication of a high gain and wide bandwidth Mid-IR optical amplifier, that could be integrated into an all-in-fiber system operating in the Mid-IR range, are provided. The considered rare earth doped fiber is feasible since it is available on market with a higher concentration. The all-in-fiber system could include commercial fiber pumping lasers (e.g., erbium doped fiber), and Mid-IR devices such as combiners or couplers that have been recently designed and realized [17], [18]. The work is presented as follows: a summary

Received 3 October 2024; revised 20 February 2025; accepted 25 February 2025. Date of publication 4 March 2025; date of current version 2 June 2025. This work was supported in part by Project H2020-ICT-37-2020 "Photonic Accurate and Portable Sensor Systems Exploiting Photo-Acoustic and Photo-Thermal Based Spectroscopy for Real-Time Outdoor Air Pollution Monitoring – PASSEPARTOUT" under Grant 101016956, in part by the European Union under the Italian National Recovery and Resilience Plan (NRRP) of NextGenerationEU, "Telecommunications of the Future" under Grant PE00000001 - Program "RESTART" and Grant CUP D93C22000910001, in part by Project DREAMS – "Antennas & Devices foR mixing, dEtection And Manipulation of mmWaves", in part by the MIUR PRIN 2022, NRRP "InnoVative tEchnoloGies for non-invasivE assessmenT of plAnt healTh conditIon to support precisiOn farmiNg – VEGETATION" – DD under Grant 1181 del 27-07-2023, in part by the Starting Grant of Politecnico di Torino under Grant 51 RIF20ST, and in part by the "Attrazione e retenzione di docenti di qualità" di Intesa Sanpaolo S.p.A under Grant 51 RSG20ST. *(Corresponding author: Francesco Prudenzano.)*

Antonella Maria Loconsole, Vito Vincenzo Francione, Francesco Anelli, and Francesco Prudenzano are with the Department of Electrical and Information Engineering at Politecnico di Bari, 70125 Bari, Italy (e-mail: antonellamaria.loconsole@poliba.it; v.francione@phd.poliba.it; francesco.anelli@poliba.it; francesco.prudenzano@poliba.it).

Stefano Taccheo is with the Department of Electronics and Telecommunications at Politecnico di Torino, Corso Duca degli Abruzzi, 24, 10129 Torino, Italy (e-mail: stefano.taccheo@polito.it).

Color versions of one or more figures in this article are available at https://doi.org/10.1109/JLT.2025.3547482.

Digital Object Identifier 10.1109/JLT.2025.3547482

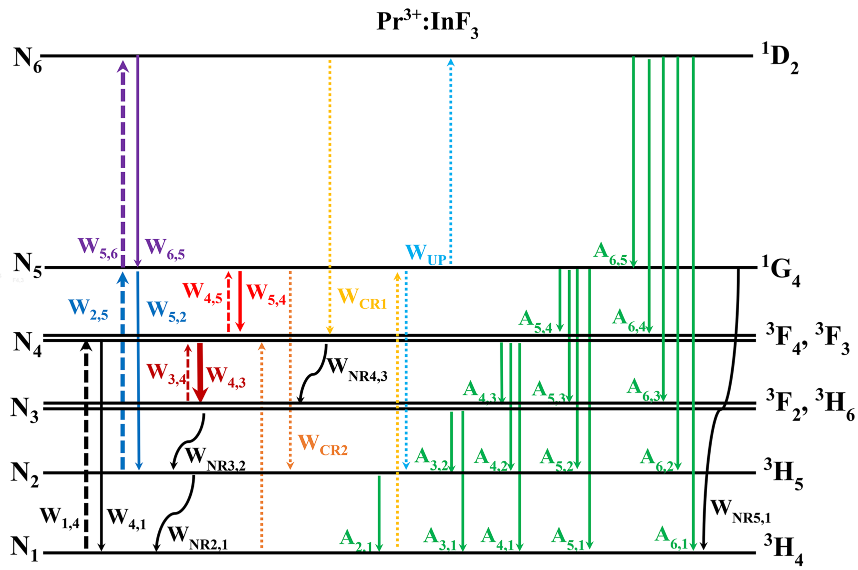

Fig. 1. Six-levels energy diagram of Pr^{3+}:InF_3 glass: pump absorption (dashed black arrow), stimulated emission at $\lambda_s = 4\ \mu$m (solid dark red arrow), stimulated emission at $\lambda_s = 3.56\ \mu$m (solid red arrow), radiative (solid green arrows) and non-radiative (curve black arrows) emissions, Excited State Absorption (ESA) (dashed blue and violet arrows), up-conversion (UP) (light-blue dotted arrows) and cross-relaxation (CR) (orange and yellow dotted arrows).

of the employed theory of the optical amplifier is reported in Section II; the amplifier model and the parameter employed in the design are reported in Section III; the model validation is reported in Section IV; the main results useful for fabrication are reported in Section V; and the conclusions are reported in Section VI.

II. Fiber Optic Amplifier Model

Fig. 1 shows the complete five-levels energy diagram and the energy transitions of the Pr^{3+}:InF_3. The fiber is pumped at wavelength $\lambda_p = 1550$ nm, and emits in the band around wavelength $\lambda_s = 4\ \mu$m. The emission phenomena to be considered are depicted with solid arrows, while the absorption phenomena are depicted with dashed arrows. In the Pr^{3+}:InF_3 energy diagram the following energy transitions are considered: i) pump absorption, ii) stimulated emission, iii) radiative and nonradiative emissions, iv) Excited State Absorption (ESA), v) up-conversion (UP) and vi) cross-relaxation (CR) phenomena [32], [34]. To solve the ions concentration of each energy level $N_1, \ldots, N_6$, the following rate equations system can be written:

$$
\begin{aligned}
\frac{\partial N_1}{\partial t} =& -W_{14}N_1 + W_{41}N_4 + A_{61}N_6 + A_{51}N_5 + A_{41}N_4 \\
&+ A_{31}N_3 + A_{21}N_2 - W_{CR1}N_6N_1 - W_{CR2}N_1N_5 \\
&+ W_{NR51}N_5 + W_{NR21}N_2 \\
\frac{\partial N_2}{\partial t} =& -W_{25}N_2 + W_{52}N_5 - \frac{1}{\tau_2}N_2 + A_{62}N_6 + A_{52}N_5 \\
&+ A_{42}N_4 + A_{32}N_3 + W_{CR2}N_1N_5 + W_{UP}N_5^2 \\
&+ W_{NR32}N_3 - W_{NR21}N_2 \\
\frac{\partial N_3}{\partial t} =& -W_{34}N_3 + W_{43}N_4 - \frac{1}{\tau_3}N_3 + A_{63}N_6 + A_{53}N_5 \\
&+ A_{43}N_4 - W_{NR32}N_3 + W_{NR43}N_4 \\
\frac{\partial N_4}{\partial t} =& W_{14}N_1 - W_{41}N_4 - W_{43}N_4 + W_{34}N_3 + W_{54}N_5 \\
&- W_{45}N_4 - \frac{1}{\tau_4}N_4 + A_{64}N_6 \\
&+ A_{54}N_5 + W_{CR1}N_6N_1 + W_{CR2}N_1N_5 - W_{NR43}N_4 \\
\frac{\partial N_5}{\partial t} =& W_{25}N_2 - W_{52}N_5 + W_{65}N_6 - W_{56}N_5 - W_{54}N_5 \\
&+ W_{45}N_4 - \frac{1}{\tau_5}N_5 + A_{65}N_6 + W_{CR1}N_6N_1 \\
&- W_{CR2}N_1N_5 - 2W_{UP}N_5^2 - W_{NR51}N_5 \\
\frac{\partial N_6}{\partial t} =& -W_{65}N_6 + W_{56}N_5 - \frac{1}{\tau_6}N_6 \\
&- W_{CR1}N_6N_1 + W_{UP}N_5^2
\end{aligned} \tag{1}
$$

where $A_{i.j}$ and $W_{NRi.j}$, are the spontaneous radiative and non-radiative decays between the i-th and j-th levels, respectively; τ_i is the lifetime of the i-th level; and W_{CR} is the cross-relaxation rate.

The pump $W_{i,j}^p$, the signal $W_{i,j}^s$ and the Amplified Spontaneous Emission (ASE) $W_{i,j}^{ASE}$ transition rates are defined by the following equations:

$$
\begin{aligned}
W_{i,j}^{p,s}(z) &= \frac{\sigma_{i,j}(\lambda_{p,s})}{hc_0/\lambda_{p,s}} \frac{\Gamma_{p,s}(\lambda_{p,s})}{A_d} P_{p,s}(z) \\
W_{i,j}^{ASE}(z) &= \int_0^{+\infty} \frac{\sigma_{i,j}(\lambda)}{hc_0/\lambda} \frac{\Gamma(\lambda)}{A_d} S_{ASE}(z, \lambda)
\end{aligned} \tag{2}
$$

where $\sigma_{i,j}(\lambda)$ is the cross section between the i-th and j-th levels at the wavelength λ; Γ is the overlap coefficient between the doped area and the electromagnetic beam profile at the wavelength λ [3], [7], [9], [27]; h is the Planck constant, c_0 is the speed of light in vacuum; A_d is the core doped area; $P_{p,s}(z)$ is the pump or signal pump; $S_{ASE}(z,\lambda)$ is the ASE power spectrum density.

The rate equations system (1) can be solved in steady state conditions, considering the conservation of ions concentration $N_1 + N_2 + N_3 + N_4 + N_5 + N_6 = N_{Pr}$.

The following three equations have been considered to model the pump power, the signal power, and the ASE power spectral density as a function of the fiber length z:

$$\frac{\partial P_p}{\partial z} = \{g_p(\lambda_p) - \alpha(\lambda_p)\} P_p(z)$$
$$\frac{\partial P_s}{\partial z} = \{g_s(\lambda_s) - \alpha(\lambda_s)\} P_s(z)$$
$$\frac{\partial S^{\pm}_{ASE}}{\partial z} = \pm\{[-\sigma_{34}(\lambda) N_3(z) + \sigma_{43}(\lambda) N_4(z) - \sigma_{45}(\lambda) N_4(z) + \sigma_{54}(\lambda) N_5(z)]\Gamma(\lambda) - \alpha(\lambda)\} \cdot S^{\pm}_{ASE}(\lambda, z) \pm a_{sp}(\lambda) \quad (3)$$

where $S^{\pm}_{ASE}(\lambda, z)$ are the forward (+) and backward (−) ASE power spectral density along the fiber; g_p and g_s are the gain coefficients for the pump and the signal; and $a_{sp}(\lambda) = 2hc_0/\lambda\,(\sigma_{43}(\lambda)N_4(z) + \sigma_{54}(\lambda)N_5(z))\Gamma(\lambda)$ is the spontaneous emission term. The overlap coefficient for the i-th wavelength $\Gamma(\lambda_i)$ is defined by following expression:

$$\Gamma(\lambda_i) = \frac{\int_{A_d} |E_i(x,y)|^2 dx\, dy}{\int_A |E_i(x,y)|^2 dx\, dy} \quad (4)$$

where $E_i(x,y)$ is the distribution of the electric field in the doped cross-section area A_d and in the total cross-section area A.

The gain coefficient for the pump g_p and for the signal g_s are defined as

$$g_p = [-\sigma_{14}(\lambda_p) N_1(z) + \sigma_{41}(\lambda_p) N_4(z) - \sigma_{25}(\lambda_p) N_2(z) + \sigma_{52}(\lambda_p) N_5(z) - \sigma_{56}(\lambda_p) N_5 + \sigma_{65}(\lambda_p) N_6]\Gamma_p$$
$$g_s = [-\sigma_{34}(\lambda_s) N_3(z) + \sigma_{43}(\lambda_s) N_4(z) - \sigma_{45}(\lambda_s) N_4(z) + \sigma_{54}(\lambda_s) N_5(z)]\Gamma_s \quad (5)$$

To solve the differential (1) the following conditions are imposed:

$$P_p(0) = P_{p0}$$
$$P_s(0) = P_{s0}$$
$$S_{ASE}{}^{+}(0,\lambda) = 0$$
$$S_{ASE}{}^{-}(L,\lambda) = 0 \quad (6)$$

Finally, the gain G and the noise figure NF for small signal operation of the fiber optic amplifier are defined by the following equations:

$$G = \frac{P_s(L)}{P_s(0)}$$
$$NF = 10\log\left(\frac{1}{G}\left(1 + \frac{S_{ASE}{}^{+}(L,\lambda_s)}{hc_0/\lambda_s}\right)\right) \quad (7)$$

III. Fiber Optic Amplifier Design

The fiber considered in the design of the optical amplifier is a single mode fluoroindate praseodymium-doped fiber. It is available on market, even if with a higher concentration [33]. To reduce the drawbacks related to the ion-ion interactions, the concentration quenching, and the glass cracking/crystallizations, a lower dopant concentration is considered. The fiber has a double cladding, with the following geometric parameters: core diameter $d_{co} = 7.5\ \mu$m, inner cladding diameter $d_{cl1} = 125\ \mu$m, outer cladding diameter $d_{cl2} = 180\ \mu$m. The inner cladding has a 2-D shape, obtained by making a cut at distance $d = 115\ \mu$m. The praseodymium concentration is fixed at $N_{Pr} = 2000$ ppm. The refractive index dispersion for fluoroindate glass has been taken from [18], [33]. The refractive index of the core, inner cladding, and outer cladding at pump wavelength $\lambda_p = 1.55\ \mu$m are $n_{co}(\lambda_p) = 1.4881$, $n_{cl,in}(\lambda_p) = 1.4746$, and $n_{cl,out}(\lambda_p) = 1.3872$, respectively. The refractive index of the core, the inner cladding and the outer cladding at central wavelength of the signal $\lambda_s = 4\ \mu$m are $n_{co}(\lambda_s) = 1.4721$, $n_{cl,in}(\lambda_s) = 1.4585$, and $n_{cl,out}(\lambda_s) = 1.3785$, respectively. The fiber exhibits a monomodal behavior at both pump wavelength $\lambda_p = 1.55\ \mu$m and signal wavelength $\lambda_s = 4\ \mu$m. The attenuation coefficient for the pump and signal is chosen equal to $\alpha = 0.2$ dB/m. This value is higher than the actual one, thus chosen in precautionary way [33].

The electromagnetic investigation of the fiber has been performed via a Finite Element Method (FEM) software. In particular, the modal analysis of the fiber has been carried out to calculate the modal propagation constants, the electromagnetic field profiles and the overlapping coefficient for the pump and the signal $\Gamma_{p,s}$. The pump overlap coefficient is $\Gamma_p = 0.899$ at wavelength $\lambda_p = 1.55\ \mu$m. The overlap coefficient of the signal decreases almost linearly with the wavelength, from $\Gamma_s = 0.57$ at $\lambda_s = 3\ \mu$m to $\Gamma_s = 0.21$ at $\lambda_s = 4.5\ \mu$m.

The design has been performed with a home-made code solver, employing the spectroscopical parameters of Table I [32], [34], [35], [36], [37]. The developed computer code solves the rate-equations system and power propagation equations for the pump, the signal, and the backward and the forward ASE noise. It has been validated with experimental results taken from literature [32]. The validation is reported in Section IV.

Fig. 2 shows the absorption and emission cross section for fluoroindate glass between the $F_{4,3} \rightarrow H_6$ levels (blue lines) and $G_4 \rightarrow F_{4,3}$ (black lines) levels. The emission cross section (solid curves) is taken from literature [32], while the absorption cross sections (dashed curves) are calculated with McCumber equation [32], [38]. The absorption cross-section calculated at the wavelength $\lambda_s = 4\ \mu$m is in agreement with the value reported in [32]. The absorption cross section values for the pump between the $H_4 \rightarrow F_{4,3}$ levels, and the emission cross section for the ESA between the $G_4 \rightarrow H_5$ levels and the $D_2 \rightarrow G_4$ are taken from the literature [9], [37], [39], [40], [41].

In the design of the optical amplifier, several simulations have been performed. Gain and noise figure have been investigated as function of input signal power P_s, input pump power P_p, fiber length L, and signal wavelength λ_s. The pump wavelength λ_p is

TABLE I
PR3+:INF3 GLASS SPECTROSCOPICAL PARAMETERS

Symbol	Value	Description	Reference
τ_2	$79\ ms$	H_5 Energy level lifetime	[34]
τ_3	$57\ ms$	H_6 Energy level lifetime	[34]
τ_4	$2.28\ ms$	$F_{4,3}$ Energy level lifetime	[32]
τ_5	$2.35\ ms$	G_4 Energy level lifetime	[32]
τ_6	$0.41\ ms$	D_2 Energy level lifetime	[37]
A_{21}	$12.63\ s^{-1}$	Radiative rate $H_5 \rightarrow H_4$	[32]
A_{31}	$10.92\ s^{-1}$	Radiative rate $H_6 \rightarrow H_4$	[34, 35]
A_{32}	$6.63\ s^{-1}$	Radiative rate $H_6 \rightarrow H_5$	[34, 35]
A_{41}	$276.58\ s^{-1}$	Radiative rate $F_{4,3} \rightarrow H_4$	[32]
A_{42}	$121.54\ s^{-1}$	Radiative rate $F_{4,3} \rightarrow H_5$	[32]
A_{43}	$40.53\ s^{-1}$	Radiative rate $F_{4,3} \rightarrow H_6$	[32]
A_{51}	$24.72\ s^{-1}$	Radiative rate $G_4 \rightarrow H_4$	[32]
A_{52}	$260.68\ s^{-1}$	Radiative rate $G_4 \rightarrow H_5$	[32]
A_{53}	$120.60\ s^{-1}$	Radiative rate $G_4 \rightarrow F_2, H_6$	[32]
A_{54}	$19.45\ s^{-1}$	Radiative rate $G_4 \rightarrow F_{4,3}$	[32]
A_{61}	$800\ s^{-1}$	Radiative rate $D_2 \rightarrow H_4$	[37]
A_{62}	$14\ s^{-1}$	Radiative rate $D_2 \rightarrow H_5$	[37]
A_{63}	$840\ s^{-1}$	Radiative rate $D_2 \rightarrow F_2, H_6$	[37]
A_{64}	$555\ s^{-1}$	Radiative rate $D_2 \rightarrow F_{4,3}$	[37]
A_{65}	$230\ s^{-1}$	Radiative rate $D_2 \rightarrow G_4$	[37]
W_{NR21}	$499987\ s^{-1}$	Non-radiative rate $H_5 \rightarrow H_4$	[34]
W_{NR32}	$6664\ s^{-1}$	Non-radiative rate $H_6 \rightarrow H_5$	[35]
W_{NR43}	$7305\ s^{-1}$	Non-radiative rate $F_{4,3} \rightarrow H_6$	[35]
W_{NR51}	$14514\ s^{-1}$	Non-radiative rate $G_4 \rightarrow H_4$	[36]
W_{CR1}	$1800\ s^{-1}$	Cross relaxation 1 rate	[34]
W_{CR2}	$2670\ s^{-1}$	Cross relaxation 2 rate	[34]
W_{UP}	$47\ s^{-1}$	Up-conversion rate	[34]

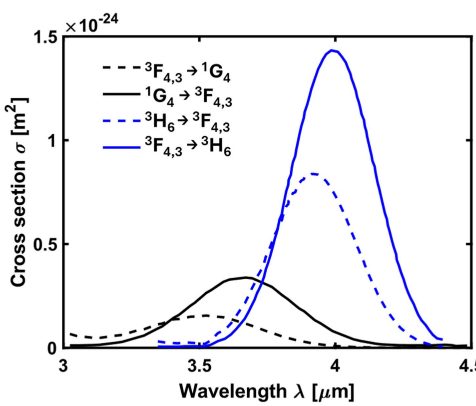

Fig. 2. Cross sections of Pr^{3+}:InF_3 glass as a function of the wavelength, for emission $F_{4,3} \rightarrow H_6$ (blue solid curve) [32], emission $G_4 \rightarrow F_{4,3}$ (black solid curve) [32], absorption $H_6 \rightarrow F_{4,3}$ calculated via McCumber equation (blue dashed curve), and absorption $F_{4,3} \rightarrow G_4$ calculated via McCumber equation (black dashed curve).

fixed at $\lambda_p = 1.55\ \mu$m, in order to consider a low-cost feeding diode eventually pumping an erbium doped fiber laser.

IV. MODEL VALIDATION

For the validation of the home-made solver, the measured emission intensity I_e at signal wavelength $\lambda_s = 4\ \mu$m for the bulk glass, reported in [32], has been considered. As reported in previous works, it is possible to compare the emission intensity I_e with the gain coefficient g_s [7], [42]. For a proper comparison, they are normalized with respect to their maximum value,

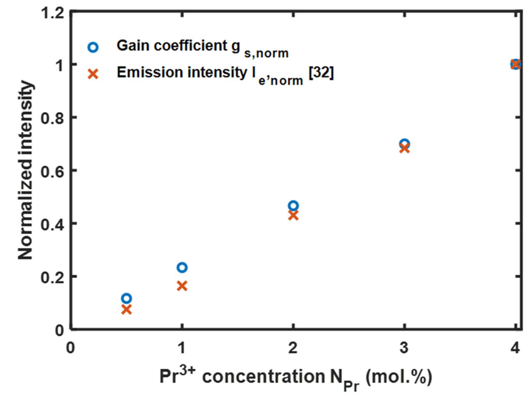

Fig. 3. Measured normalized emission intensity $I_{e,norm}$ (red crosses) [32] and simulated normalized gain coefficient $g_{s,norm}$ (blue circles) at signal wavelength $\lambda_s = 4\ \mu$m as a function of the dopant concentration N_{Pr}.

obtained at $N_{Pr} = 4000\ ppm$. The gain coefficient g_s has been calculated, see (5), at signal wavelength $\lambda_s = 4\ \mu$m for different concentrations of praseodymium N_{Pr}, and normalized.

Fig. 3 shows the measured normalized emission intensity $I_{e,norm}$ (red crosses) [32] and the simulated normalized gain coefficient $g_{s,norm}$ (blue circles) at signal wavelength $\lambda_s = 4\ \mu$m as a function of the dopant concentration N_{Pr}. All the points are in good agreement, confirming the good approach of the model.

Similar solver codes, based on the rate equation approach, have been employed for the design of a number of optical devices. As examples: i) CW and pulsed lasers based on a holmium-doped fluoroindate fiber, providing results comparable with experimental results taken from literature [3], [7]; ii) a CW laser based on praseodymium-doped fluoroindate fiber [9]; iii) a MOPA amplifier based on a dysprosium-doped chalcogenide fiber [27]; iv) a CW laser based on an erbium-doped fluoroindate fiber [43].

V. DESIGN AND RESULT DISCUSSION

The optical amplifier is designed to operate at the signal wavelength $\lambda_s = 4\ \mu$m, considering dopant concentration $N_{Pr} =$ 2000 ppm, and pump wavelength $\lambda_p = 1.55\ \mu$m.

Fig. 4 shows the amplifier gain G as a function of input signal power P_s for different values of input pump power $P_p = 0.5$ W (solid curve), $P_p = 1$ W (dashed curve), $P_p = 2$ W (dot-dashed curve) and $P_p = 3$ W (dotted curve), for the fiber length $L = 3$ m and signal wavelength $\lambda_s = 4\ \mu$m. The saturation input signal power $P^{in}_{s,sat}$, limiting the amplifier linear behavior, is defined as the input signal power where the gain G drops of -3 dB below its unsaturated value [42], [43]. It decreases by increasing the input pump power P_p it being $P^{in}_{s,sat} = 8$ dBm, $P^{in}_{s,sat} = -1.5$ dBm, $P^{in}_{s,sat} = -14.7$ dBm, $P^{in}_{s,sat} = -14.8$ dBm, for the input pump power of $P_p = 0.5$ W, $P_p = 1$ W, $P_p = 2$ W, and $P_p = 3$ W, respectively.

Fig. 5 shows the gain G as a function of input signal power P_s for different values of fiber length $L = 1$ m (solid curve), $L = 2$ m (dashed curve), and $L = 3$ m (dot-dashed curve), for input pump power $P_p = 2$ W. The saturation input signal power decreases when the fiber length L is increased. In particular, for

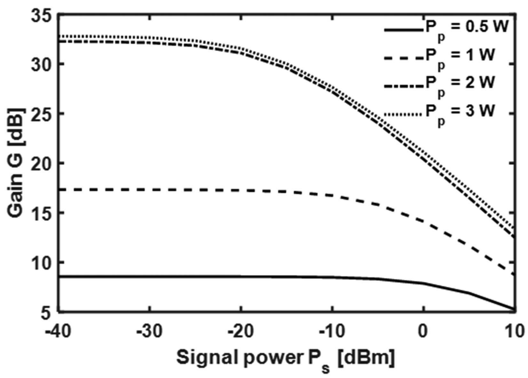

Fig. 4. Gain G as a function of input signal power P_s, for different values of input pump power $P_p = 0.5$ W (solid curve), $P_p = 1$ W (dashed curve), $P_p = 2$ W (dot-dashed curve) and $P_p = 3$ W (dotted curve), for the fiber length $L = 3$ m, and signal wavelength $\lambda_s = 4$ μm.

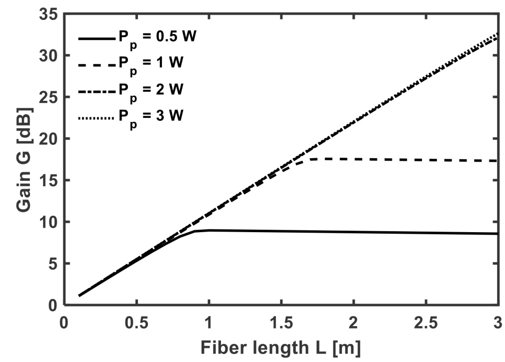

Fig. 7. Gain G as function of fiber length L, for input pump power $P_p = 0.5$ W (solid curve), $P_p = 1$ W (dashed curve), $P_p = 2$ W (dot-dashed curve), and $P_p = 3$ W (dotted curve), for input signal power $P_s = -30$ dBm, signal wavelength $\lambda_s = 4$ μm.

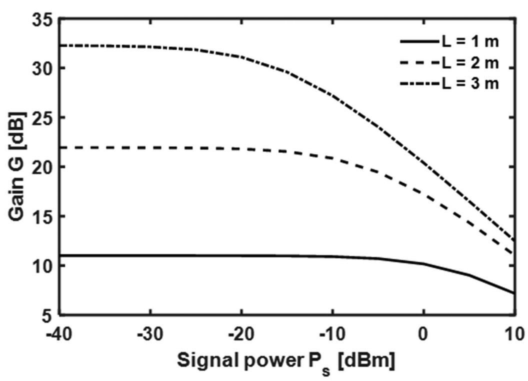

Fig. 5. Gain G as a function of input signal power P_s for fiber length $L = 1$ m (solid curve), $L = 2$ m (dashed curve), $L = 3$ m (dot-dashed curve), for input pump power $P_p = 2$ W, and signal wavelength $\lambda_s = 4$ μm.

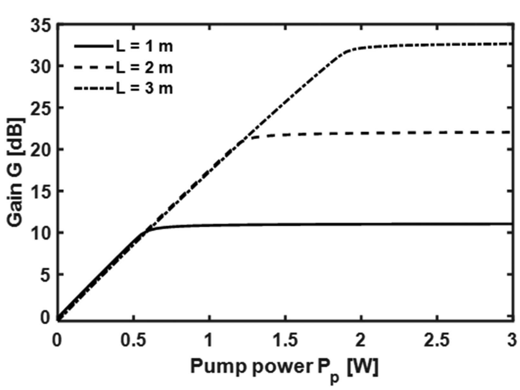

Fig. 6. Gain G as function of input pump power P_p, for fiber length $L = 1$ m (solid curve), $L = 2$ m (dashed curve), and $L = 3$ m (dot-dashed curve), for input signal power $P_s = -30$ dBm, and signal wavelength $\lambda_s = 4$ μm.

$L > 3$ m, the characteristic becomes quite linear. Therefore, in the next simulations, fiber length $L = 3$ m has been considered an upper limit and an input signal power of $P_s = -30\ dBm$ has been chosen, in order to work in linear small-signal regime.

Fig. 6 shows the gain G as a function of input pump power P_p for different values of fiber length $L = 1$ m, (solid curve), $L = 2$ m (dashed curve), $L = 3$ m (dot-dashed curve), for input signal power $P_s = -30$ dBm. There are three pumping ranges: the under pumped regime($P_p < P_{p,inv}$) where the population inversion is not reached, the non-complete inversion regime ($P_p > P_{p,inv}$), and the complete inversion regime ($P_p \gg P_{p,inv}$) [38], [44], [45]; therefore $P_{p,lin} = 0.6$ W is the minimum value allowing the correct operation for the fiber length $L = 1$ m.

Fig. 7 shows the gain G as function fiber length L for different value of the input pump power $P_p = 0.5$ W (solid curve), $P_p = 1$ W (dashed curve), $P_p = 2$ W (dot-dashed curve), and $P_p = 3$ W (dotted curve), for input signal power $P_s = -30$ dBm. The gain reaches a maximum value and then slightly decreases for increasing fiber length.

Fig. 8 shows (a) the gain G and (b) the noise figure NF as a function of the input signal wavelength λ_s for different value of the input pump power $P_p = 0.5$ W (solid curve), $P_p = 1$ W (dashed curve), $P_p = 2$ W (dot-dashed curve), and $P_p = 3$ W (dotted curve), for fiber length $L = 3$ m. The maximum gain at the central wavelength $\lambda_s = 4$ μm is $G = 8.57$ dB, $G = 17.32$ dB, $G = 32.6$ dB, and $G = 32.65$ dBm, for input pump power $P_p = 0.5$ W, $P_p = 1$ W, $P_p = 2$ W, and $P_p = 3$ W, respectively. The bandwidth, calculated at $-3dB$, decreases from $B_{-3dB} = 220$ nm for $P_p = 0.5$ W to $B_{-3\,\mathrm{dB}} = 95$ nm for $P_p = 3$ W. The noise figure NF decreases in the range $\lambda_s = 3.5 - 4.5$ μm. In the wavelength range $\lambda_s = 3.5 - 3.8$ μm, the spontaneous emission phenomenon between the levels $G_4 \rightarrow F_{4,3}$ dominates the other phenomena, and this increases the noise figure in this range. In the wavelength range $\lambda_s = 3.8 - 4.2$ μm, the noise figure is about $NF = 6.3$ dB. In the wavelength range $\lambda_s = 4.2 - 4.5$ μm, the noise figure NF is less then quantum limit ($NF < 3$ dB) [38], [44], [45].

Fig. 9 shows (a) the gain G, and (b) the noise figure NF as function of input signal wavelength λ_s for different fiber length $L = 1$ m (solid curve), $L = 2$ m (dashed curve), $L = 3$ m (dot-dashed curve). An input pump power $P_p = 2$ W is chosen in order to work with complete population inversion. The maximum gain at the central wavelength $\lambda_s = 4$ μm is $G = 11$ dB, $G = 21.93$ dB, and $G = 32.14$ dB, for fiber length $L = 1$ m, $L = 2$ m, and $L = 3$ m, respectively. The bandwidth, calculated at -3 dB, varies from $B_{-3\,\mathrm{dB}} = 165$ nm for $L = 1$ m to

TABLE II
COMPARISON BETWEEN OPTICAL AMPLIFIERS WORKING IN MID-IR AND NIR

Ref.	Glass	Dopant	Pump wavelength λ_p $[\mu m]$	Central emission wavelength λ_s $[\mu m]$	Input pump Power P_p $[W]$	Input signal power P_s $[dBm]$	Gain G $[dB]$	Bandwidth B_{-3dB} $[nm]$
[22]	ZBLAN	Er^{3+}	0.98	2.7	12.5	~18	15.4	250
[23]	ZFG	Er^{3+}	0.98	2.8	9.63	~13	> 20	95
[24]	ZFG	Er^{3+}	0.98	2.79	5.8	~7.2	20	22
[25], [26]	Chalcogenide	Pr^{3+}	1.55	4.3	0.37	−20	> 30	–
[26]	Chalcogenide	Dy^{3+}	1.3	4.4	0.26	−13	> 15	–
[26]	Chalcogenide	Tb^{3+}	2.0	4.9	0.28	−13	> 25	–
[27]	Chalcogenide	Dy^{3+}	1.71	4.4	3	0	$25 - 28$	–
[28]	Chalcogenide	Er^{3+}	0.98	2.8	0.1	−50	33.7	–
This work	InF_3	Pr^{3+}	1.55	4.0	2	−30	> 30	130

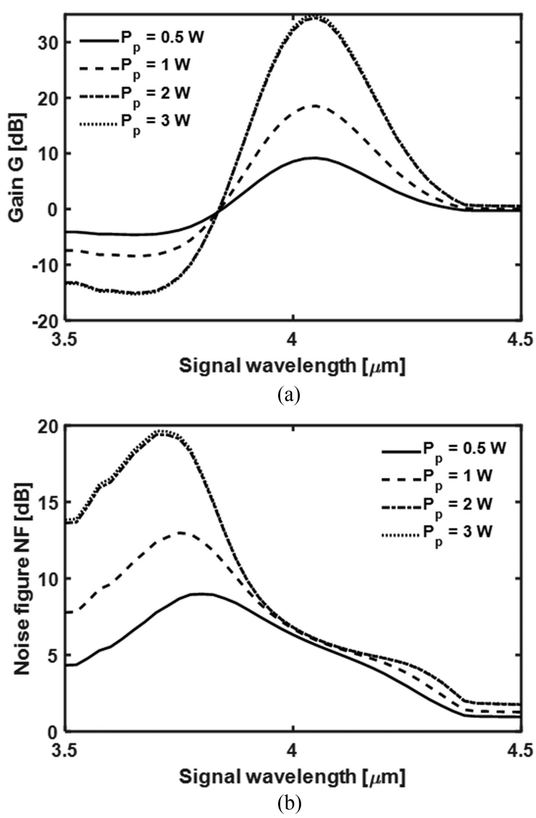

Fig. 8. (a) Gain G, and (b) noise figure NF as function of input signal wavelength λ_s, for input pump power $P_p = 0.5$ W (solid curve), $P_p = 1$ W (dashed curve), $P_p = 2$ W (dot-dashed curve), and $P_p = 3$ W (dotted curve), for input signal power $P_s = -30$ dBm, and fiber length $L = 3$ m.

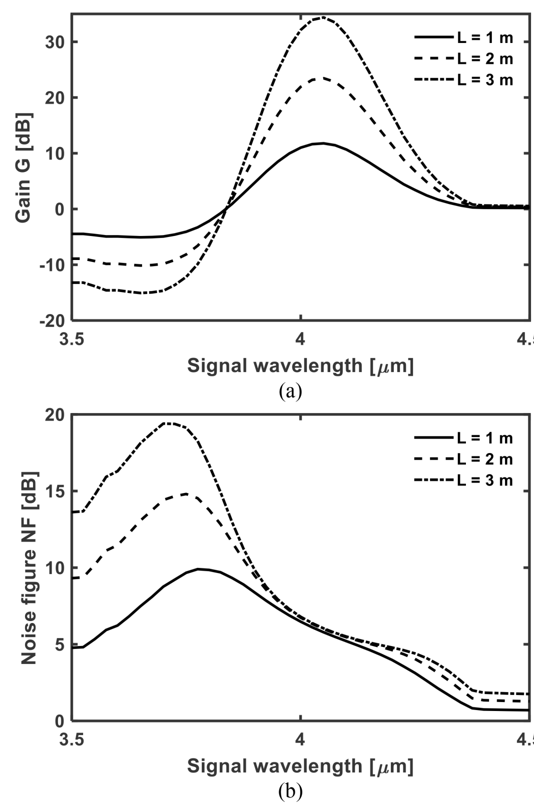

Fig. 9. (a) Gain G, and (b) noise figure NF as function of input signal wavelength λ_s for different fiber length $L = 1$ m (solid curve), $L = 2$ m (dashed curve), $L = 3$ m (dot-dashed curve), for input signal power $P_s = -30$ dBm, input pump power $P_p = 2$ W.

$B_{-3\,\mathrm{dB}} = 110$ nm for $L = 3$ m. The noise figure NF decreases in the range $\lambda_s = 3.5 - 4.5$ μm. We note that we achieve gain $G > 30$ dB in a wavelength range of over $B = 130$ nm with noise figure $NF = 6$ dB.

The optimized amplifier exhibits gain $G = 32.1$ dB, bandwidth $B_{-3\,\mathrm{dB}} = 115$ nm, and small signal regime till $P_s^{in} = -14.7$ dBm for input pump power $P_p = 2$ W and fiber length $L = 3$ m. Table II reports a comparison between the fiber optical amplifier proposed in this work, and other optical amplifiers from literature [22], [23], [24], [25], [26], [27], [28]. The comparison takes into account the dopant ion, the pump wavelength λ_p, the central emission wavelength λ_S, the input pump power P_p, the input signal power P_s, the gain G, and the bandwidth around the central wavelength $B_{-3\,\mathrm{dB}}$, calculated at -3 dB. Compared to other fluoride fiber amplifiers, the one proposed in this work operates in the wavelength range around $\lambda_s = 4$ μm with one of the widest bandwidths, the lowest input pump power and a good gain. Amplification around similar central emission wavelengths has been obtained only with chalcogenide fibers with much higher input pump powers.

VI. CONCLUSION

In this paper for the first time to the best of our knowledge, a Mid-IR optical amplifier based on a fluoroindate fiber doped with praseodymium (Pr^{3+}:InF_3) has been designed. The behavior of the optical amplifier has been investigated as a function of different input parameters. It works at central wavelength $\lambda_s = 4\,\mu$m, when pumped at $\lambda_p = 1.55\,\mu$m. The amplifier proves high gain $G = 32.1$ dB, noise figure $NF = 6\,dB \pm 0.2$ dB and wide bandwidth $B_{-3dB} = 115$ nm, for input pump power $P_p = 2\,W$, fiber length $L = 3$ m, and input signal power $P_s = -30$ dBm. The bandwidth above 30 dB gain is $B = 130$ nm. An all-in-fiber amplifier could be based on commercial fiber pumping lasers (e.g., erbium doped fiber), and the illustrated design, obtaining high gain and wide bandwidth amplifier working in the Mid-IR.

References

[1] C. Wei et al., "Mid-infrared Q-switched and mode-locked Fiber lasers at 2.87 μm based on carbon nanotube," *IEEE J. Sel. Topics Quantum Electron.*, vol. 25, no. 4, Jul./Aug. 2019, Art. no. 1100206.

[2] O. Henderson-Sapir et al., "Mode-locked and tunable 3.5 μm fiber laser using an acousto-optic modulator," *J. Lightw. Technol.*, vol. 41, no. 2, pp. 716–725, Jan. 2023.

[3] A. M. Loconsole, M. C. Falconi, V. Portosi, and F. Prudenzano, "Numerical design of a gain-switched pulsed laser at 3.92 μm wavelength based on a Ho^{3+}-doped fluoroindate fiber," *J. Lightw. Technol.*, vol. 39, no. 10, pp. 3276–3283, May 2021.

[4] J. J. Nunes et al., "Room temperature mid-infrared fiber lasing beyond 5 µm in chalcogenide glass small-core step index fiber," *Opt. Lett.*, vol. 46, pp. 3504–3507, Jul. 2021.

[5] F. Maes et al., "Room-temperature fiber laser at 3.92 μm," *Optica*, vol. 5, pp. 761–764, 2018.

[6] M. Federico and F. Poli, "Numerical optimization of Dy-doped ZBLAN fiber lasers for yellow emission," *J. Lightw. Technol.*, vol. 42, no. 7, pp. 2480–2487, 2024.

[7] A. M. Loconsole, M. C. Falconi, A. Annunziato, S. Cozic, S. Poulain, and F. Prudenzano, "Design of a mid-IR laser based on a Ho:Nd-codoped fluoroindate fiber," *J. Lightw. Technol.*, vol. 41, no. 2, pp. 702–708, Jan. 2023.

[8] M. R. Majewski and S. D. Jackson, "Numerical design of 4μm -class dysprosium fluoride fiber lasers," *J. Lightw. Technol.*, vol. 39, no. 15, pp. 5103–5110, Aug. 2021.

[9] A. M. Loconsole, V. V. Francione, A. Annunziato, F. Anelli, and F. Prudenzano, "Design of a high-performance mid-IR fiber laser based on Pr^{3+}-doped fluoroindate glass," *J. Lightw. Technol.*, vol. 42, no. 7, pp. 2488–2493, Apr. 2024.

[10] Z. Cheng et al., "Numerical modeling of dual-wavelength pumped heavily-Ho^{3+}-doped fluoroindate fiber lasers with efficient output at 3.92 μm," *J. Lightw. Technol.*, vol. 41, no. 22, pp. 7021–7028, Nov. 2023.

[11] M. Michalska, J. Mikolajczyk, J. Wojtas, and J. Swiderski, "Mid-infrared, super-flat, supercontinuum generation covering the 2–5 μm spectral band using a fluoroindate fibre pumped with picosecond pulses," *Sci. Reports*, vol. 6, no. 39138, Dec. 15 2016.

[12] J. C. Gauthier et al., "Mid-IR supercontinuum from 2.4 to 5.4 μm in a low-loss fluoroindate fiber," *Opt. Lett.*, vol. 41, pp. 1756–1759 2016.

[13] G. Scurria, I. Manek-Hönninger, J. Y. Carré, A. Hildenbrand-Dhollande, and S. Bigotta, "7 W mid-infrared supercontinuum generation up to 4.7 μm in an indium-fluoride optical fiber pumped by a high-peak power thulium-doped fiber single-oscillator," *Opt. Exp.*, vol. 28, pp. 7672–7677, Jan. 2020.

[14] G. Ricchiuti, A. Dabrowska, D. Pinto, G. Ramer, and B. Lendl, "Dual-beam photothermal spectroscopy employing a Mach−Zehnder interferometer and an external cavity quantum cascade laser for detection of water traces in organic solvents," *Anal. Chem.*, vol. 94, pp. 16353–16360, Nov. 2022.

[15] B. Behzadi and M. Hossein-Zadeh, "On the performance of intracavity gas sensors based on whispering-gallery microlasers," *IEEE Sensors J.*, vol. 20, no. 17, pp. 9772–9778, Sep. 2020.

[16] K. Goya, Y. Koyama, Y. Nishijima, S. Tokita, R. Yasuhara, and H. Uehara, "A fluoride fiber optics in-line sensor for mid-IR spectroscopy based on a side-polished structure," *Sensors Actuators B, Chem.*, vol. 351, Oct. 2021, Art. no. 130904.

[17] A. Annunziato, F. Anelli, P. L. Pays Du Teilleul, S. Cozic, S. Poulain, and F. Prudenzano, "Fused optical fiber combiner based on indium fluoride glass: Perspectives for mid-IR applications," *Opt. Exp.*, vol. 30, pp. 44160–44174, Nov. 2022.

[18] F. Anelli et al., "Low-loss fluoride optical Fiber coupler for mid-infrared applications," *J. Lightw. Technol.*, vol. 42, no. 7, pp. 2457–2463, Apr. 2024.

[19] S. D. Jackson and R. K. Jain, "Fiber-based sources of coherent MIR radiation: Key advances and future prospects (invited)," *Opt. Exp.*, vol. 28, pp. 30964–31019, 2020.

[20] M. Kochanowicz et al., "Near-IR and mid-IR luminescence and energy transfer in fluoroindate glasses co-doped with Er^{3+}/Tm^{3+}," *Opt. Mater. Exp.*, vol. 9, pp. 4772–4781, 2019.

[21] Ł. Sójka et al., "Mid-infrared emission from Dy3+ doped fluoroindate glass fiber," *Ceramics Int.*, vol. 49, no. 24, pp. 41210–41216, 2023.

[22] X. Zhu and R. K. Jain, "High output power (2.45 Watts) mid-IR Fiber amplifier," presented at the Opt. Fiber Commun. Conf. Expo. Nat. Fiber Optic Engineers Conf., Anaheim, CA, USA, Mar. 5–10, 2006, Paper OThJ1.

[23] Y. Wang et al., "2.3 W, linearly-polarized superfluorescent generation from a polarization-maintaining Er^{3+}-doped fluoride Fiber amplifier around 2.8 μm," *J. Lightw. Technol.*, vol. 40, no. 17, pp. 6001–6005, Sep. 2022.

[24] N. B. Chichkov et al., "Amplification of nanosecond pulses in a single-mode erbium-doped fluoride fibre amplifier," *IEEE Photon. Technol. Lett.*, vol. 35, no. 1, pp. 3–6, Jan. 2023.

[25] E. A. Anashkina and A. V. Kim, "Numerical simulation of ultrashort mid-IR pulse amplification in praseodymium-doped chalcogenide fibers," *J. Lightw. Technol.*, vol. 35, no. 24, pp. 5397–5403, Dec. 2017.

[26] E. A. Anashkina, "Design and numerical modeling of broadband mid-IR rare-earth-doped chalcogenide Fiber amplifiers," *IEEE Photon. Technol. Lett.*, vol. 30, no. 13, pp. 1190–1193, Jul. 2018.

[27] M. C. Falconi et al., "Dysprosium-doped chalcogenide master oscillator power amplifier (MOPA) for mid-IR emission," *J. Lightw. Technol.*, vol. 35, no. 2, pp. 265–273, Jan. 2017.

[28] G. Palma et al., "Design of fiber coupled Er^{3+} chalcogenide microsphere amplifier via particle swarm optimization algorithm," *Opt. Eng.*, vol. 53, no. 7, Jul. 2014, Art. no. 071805.

[29] Y. Ohishi, T. Kanamori, T. Kitagawa, S. Takahashi, E. Snitzer, and G. H. Sigel, "Pr3+-doped fluoride fiber amplifier operating at 1.31 μm," *Opt. Lett.*, vol. 16, pp. 1747–1749, Jul. 1991.

[30] Y. Miyajima, T. Sugawa, and Y. Fukasaku, "2 dB amplification at 1.31 μm and possibility of 0.98 μm pumping in Pr^{3+}-doped fluoride fibre," *Electron. Lett.*, vol. 27, pp. 1706–1707, Sep. 1991.

[31] B. Pedersen, W. J. Miniscalco, and R. S. Quimby, "Optimization of Pr^{3+}: ZBLAN Fiber amplifiers," *IEEE Photon. Technol. Lett.*, vol. 4, pp. 446–448, May 1992.

[32] H. He, Z. Jia, Y. Ohishi, W. Qin, and G. Qin, "Efficient 4 μm emission from Pr^{3+}/Yb^{3+} co-doped fluoroindate glass," *Opt. Lett.*, vol. 46, pp. 5607–5610, 2021.

[33] Le Verre Fluoré, Catalog, Bruz, Brittany, France, 2022 [Online]. Available: https://leverrefluore.com/wp-content/uploads/2022/02/LVF-Catalog-2022.pdf

[34] A. Remillieux et al., "Upconversion mechanisms of a praseodymium-doped fluoride fibre amplifier," *J. Phys. D, Appl. Phys.*, vol. 29, pp. 963–974, Jan. 1996.

[35] R. Pappalardo, "Calculated quantum yields for photon-cascade emission (PCE) for Pr^{3+} and Tm^{3+} in fluoride hosts," *J. Lumin.*, vol. 14, pp. 159–163, 1976.

[36] L. Gomes and S. D. Jackson, "Spectroscopic properties of ytterbium, praseodymium-codoped fluorozirconate glass for laser emission at 3.6 μm," *J. Opt. Soc. Amer.*, vol. 30, pp. 1410–1419, 2013.

[37] W. A. Pisarski et al., "Fluoroindate glasses co-doped with Pr^{3+}/Er^{3+} for near-infrared luminescence applications," *Sci. Reports*, vol. 10, Dec. 2020, Art. no. 21105.

[38] P. C. Becker, N. A. Olsson, and J. R. Simpson, *Erbium-Doped Fiber Amplifier: Fundamentals and Technology*, New York, NY, USA: Wiley, 2002, pp. 131–250.

[39] A. Flórez, O. L. Malta, Y. Messaddeq, and M. A. Aegerter, "Judd-Ofelt analysis of Pr^{3+} ions in fluoroindate glasses: Influence of odd third order intensity parameters," *J. Non-Crystalline Solids*, vol. 213-214, pp. 315–320, May 1997.

[40] D. Manzani, D. Pabœuf, S. J. L. Ribeiro, P. Goldner, and F. Bretenaker, "Orange emission in Pr^{3+}-doped fluoroindate glasses," *Opt. Mater.*, vol. 35, no. 3, pp. 383–386, 2013.

[41] R. S. Quimby and B. Zheng, "New excited state absorption measurement technique and application to Pr^{3+}-doped fluorozirconate glass," *Appl. Phys. Lett.*, vol. 60, pp. 1055–1057, Mar. 1992.

[42] M. C. Falconi et al., "Design of active devices based on rare-earth-doped glass/glass ceramic: From the material characterization to the device parameter refinement," *Proc. SPIE*, vol. 11357, Apr. 2020, Art. no. 1135709.

[43] M. C. Falconi, A. M. Loconsole, A. Annunziato, S. Cozic, S. Poulain, and F. Prudenzano, "Design of a broadband erbium-doped fluoroindate Fiber laser emitting up to 3.91 μm," *J. Lightw. Technol.*, vol. 41, no. 18, pp. 6065–6072, Sep. 2023.

[44] E. Desurvire, *Erbium-Doped Fiber Amplifier – Principles and Applications*. John Wiley & Sons Inc., 1994, pp. 306–452.

[45] M. J. F. Digonnet, *Rare-Earth-Doped Fiber Lasers and Amplifiers*, 2 ed., New York, NY, USA: Marcel Dekker, 1997.

Antonella Maria Loconsole received the Ph.D. degree in electrical and information engineering from Politecnico di Bari, Bari, Italy, in 2022. She is currently a Research Assistant in electromagnetic fields with the Department of Electrical and Information Engineering, Politecnico di Bari. Her research interests include optical fiber lasers and amplifiers, SIW antennas, and microwave applicators for medical applications.

Vito Vincenzo Francione received the M.Sc. degree in automation engineering (cum laude) from Politecnico di Bari, Bari, Italy, in 2021. He is currently working toward the Ph.D. degree in electrical and information engineering. His research focuses on optical and microwave devices such as laser and amplifier, antennas, and metamaterials.

Francesco Anelli received the M.Sc. degree in electronic engineering (cum laude) from Politecnico di Bari, Bari, Italy, in 2021, and the Ph.D. degree in electrical and information engineering in 2024. His research interests include the modeling and the characterization of antennas, metamaterials, optical fiber grating sensors, and optical devices for multi-spectral gas monitoring.

Stefano Taccheo received the Ph.D. degree in applied physics from Politecnico di Turin, Turin, Italy, in 1996. He was an Associate Professor with Politecnico di Milano, Milan, Italy, in 2004. He has authored more than 250 journal and conference publications. His research interests include fibre lasers, MIR-sources, spectroscopy of new glasses and active materials, solid state lasers, optical amplifiers, continuum sources, and fibre-based optical components. He has authored more than 250 journal and conference publications.

Francesco Prudenzano (Member, IEEE) received the Ph.D. degree in electronic engineering from Politecnico di Bari, Bari, Italy, in 1996. Since 2018, he has been a Full Professor in electromagnetic fields with the Department of Electrical and Information Engineering, Politecnico di Bari. From 2017 to 2018, he was the Chair of SIOF and the Italian Society of Optics and Photonics (Italian branch of EOS - European Optical Society). He is currently the Head of Microwave and Optical Engineering Group, Department of Electrical and Information Engineering, Politecnico di Bari. He is involved in several national and international research projects and cooperations. He has coauthored more than 400 publications, 295 of which got published in journals and international conferences, lectures, and invited papers. His research interests include the design and characterization of microwave devices, integrated optics, and optical fiber-based devices.